Quenched by ice: Transient grating measurements of vibronic dynamics in bromine-doped ice

I. U. Goldschleger, V. Senekerimyan, M. S. Krage, H. Seferyan,
K. C. Janda, and V. A. Apkarian[a)]
Department of Chemistry, University of California, Irvine, California 92697-2025

(Received 9 December 2005; accepted 10 April 2006; published online 25 May 2006)

In both water and in ice, the absorption spectra of bromine are dramatically broadened and blueshifted, and all fluorescence is quenched. Time resolved, electronically resonant transient grating measurements are carried out to characterize the vibronic dynamics of the trapped molecule in its electronic $B(^3\Pi_{0u})$ state in ice. Independent of the initial excitation energy, after the first half-period of motion, a vibrational packet is observed to oscillate near the bottom of the potential, near $\nu=1$. The oscillations undergo a chirped decay to a terminal frequency of 169 cm^{-1} on a time scale of $\tau_\nu=1240$ fs, to form the stationary $\nu=0$ level. The electronic population in the B state decays in $\tau_e=1500$ fs. Adiabatic following to the cage-compression coordinate is a plausible origin of the chirp. Analysis of the absorption spectrum is provided to recognize that solvent coordinates are directly excited in the process. The observed blueshift of the absorption is modeled by considering the Br_2-OH_2 complex. Two-dimensional simulations, that explicitly include the solvent coordinate, reproduce both the time data and the absorption spectrum. The observed sharp vibrational recursions can be explained by overdamped motion along the solvent coordinate, and wave packet focusing by fast dissipation during the first half-period of motion of the molecular coordinate. © *2006 American Institute of Physics*. [DOI: 10.1063/1.2201749]

I. INTRODUCTION

We report on photodynamical studies of molecular bromine isolated in ice, as part of a program aimed at investigations of clathrate hydrates,[1,2] bromine hydrate being one of the earliest discovered.[3] The concept is to use the guest chromophore as a reporter of the structure and dynamics of the crystalline clathrate host, which consists of a highly ordered lattice of water molecules. As a background to such studies, it is useful to establish the vibronic dynamics of the same chromophore in ice, since bromine-ice domains can be expected as inclusions in clathrates prepared for spectroscopic purposes. More generally, the vibronic dynamics of molecular impurities in ice are of interest. Trapped molecules in ice matrices are abundant in nature, and the understanding of the photodynamics of such trapped species is of broad relevance to atmospheric chemistry,[4,5] interstellar photophysics, and planetary compositions.[6,7]

As the title suggests, radiative transitions of bromine are strongly quenched in ice. It can be expected that the local fluctuating electric fields created by the dipolar molecular lattice points, which retain orientational disorder even at cryogenic temperatures,[8] can mix electronic states. Indeed, in the case of molecular bromine we verify that all of the commonly observed fluorescence bands are effectively quenched. As such, the ubiquitous spectroscopic tool of laser-induced fluorescence is not a viable option. We resort to electronically resonant transient grating (TG) measurements instead, to directly monitor vibronic dynamics in the excited electronic B state of bromine in ice. The all-resonant four-wave mixing scheme, which is illustrated in Fig. 1, can be implemented with selectivity and sensitivity to yield information about the excited population dynamics similar to that of pump-probe (PP) measurements using laser-induced fluorescence. While PP yields the imaginary component of the third-order polarization, $\mathrm{Im}(P^{(3)})$, homodyne detected TG measures the squared sum of real and imaginary parts, $|P^{(3)}|^2$.[9–11] The measurements allow the characterization of vibronic dissipation dynamics and energetics, which is in stark contrast with the recent pump-probe measurements of bromine in the atomic host of solid Ar.[12,13] We consider the elements that distinguish the dynamics in the molecular solid host from the model systems of molecular impurities isolated in the atomic rare gas matrices.[14]

II. EXPERIMENT

The samples are prepared by vapor deposition of the premixed gas, in the ratio of 1:500 of $Br_2:H_2O$, on a 500 μm sapphire substrate held at 120 K. A second bulb containing pure water vapor is used to cover the sample, to ensure that Br_2 does not segregate or diffuse under vacuum. Sample thicknesses were varied, in the estimated range between 10 and 150 μm, in an effort to maximize signal and minimize optical scattering. The time resolved measurements were conducted at the deposition temperature of 120 K.

The laser system used in these experiments consists of a Ti:sapphire oscillator tunable between 780 and 830 nm. The output is amplified regeneratively, to deliver 0.6 mJ energy per pulse at 1 KHz. The output is split in 90/10 ratio, with the stronger arm used to pump an optical parametric ampli-

[a)]Electronic mail: igoldshl@uci.edu

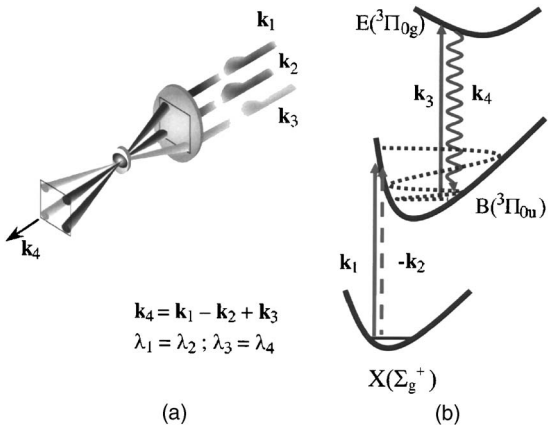

FIG. 1. Transient grating measurements, (a) the experimental geometry; (b) along the molecular coordinate, a wave packet is launched on the *B* state and probed via the ion-pair resonances. Solid and dashed arrows up define the action on *ket* and *bra*.

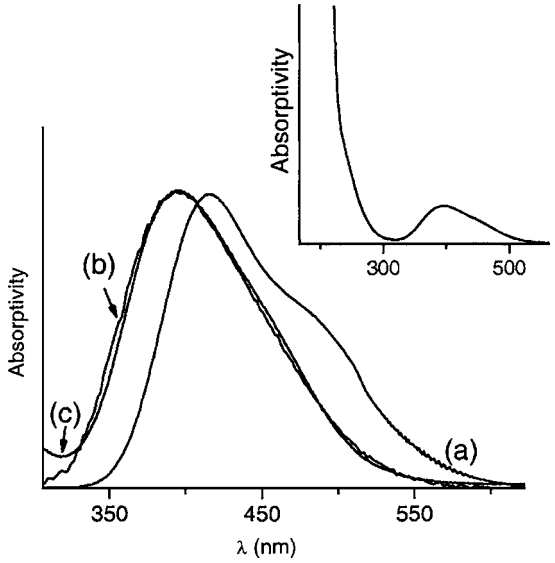

FIG. 2. UV-Vis absorption spectra of (a) the gaseous Br_2, (b) aqueous molecule, and (c) Br_2 doped ice at 1:500 doping ratio. The spectrum of the Br_2 in ice is recorded at 120 K. The strong absorption edge of the charge transfer states of guest and host in the hydrated samples is shown in the inset.

fier (Light Conversion "TOPAS") to generate tunable visible pulses. The leftover is used for second harmonic generation (SHG) in the 500 μm beta barium borate (BBO) crystal. By tuning the Ti:sapphire output SHG radiation centered at 400 or 405 nm is generated for the measurement. The optical parametric amplifier (OPA) output is compressed down to 40 fs using a pair of SF10 prisms. The spectral width of the pulses was 7 nm full width at half maximum (FWHM). The experimental time resolution is 120 fs, as measured by four-wave mixing in a 500 μm sapphire substrate in the same geometry used in the experiments. The limitation in time resolution is due to the group velocity mismatch in the BBO crystal and the group velocity dispersion in the thick achromatic lens.

The transient grating measurements are carried out using three noncollinear beams in the boxcars geometry, using a single (fl=15 cm) achromatic lens to focus onto the sample (see Fig. 1). Two coincident visible beams are used to write the optical grating, and the second harmonic of the Ti:sapphire laser is used to read the grating along $\mathbf{k}_4=\mathbf{k}_1-\mathbf{k}_2+\mathbf{k}_3$. Since $\lambda_1=\lambda_2$, energy conservation dictates that the detected radiation is at $\lambda_4=\lambda_3$, i.e., at the same color as the probe laser. Scattering of the probe laser by the ice films is the principle source of noise in the measurements. Several steps are taken to increase the signal-to-noise ratio (SNR) to a tolerable level. First, the signal is spatially filtered through an iris pinhole placed at a distance of 10 cm from the sample. Subsequently, at a distance of 3 m, the signal is tightly focused using a 5 cm lens and passed through a 25 μm pinhole prior to detection. A 1/4 monochromator, which is effective in rejecting the scattered pump light, is coupled to a photomultiplier tube (PMT) for detection. Spatial filtering alone is not sufficient. Further improvement of the SNR is obtained by synchronously chopping one of the visible beams at 500 Hz, using a phase-locked loop referenced to the pockels cell of the regenerative amplifier. The signal is then collected with a boxcar integrator operating in toggle mode (alternating polarity of the input amplifier), and averaged typically for 300 pulses. A figure of merit for the dynamic range of the measurement is the SNR obtained for the nonresonant four-wave signal, at *t*-zero, when all three input beams coincide in time. The combination of spatial filtering and common mode rejection by the chopping scheme yields a ratio of 10^4:1.

Measurements were carried out with gratings prepared at three different colors, $\lambda_1=\lambda_2=550$, 536, and 524 nm, and probed at two different colors, $\lambda_3=400$ and 405 nm. In all the reported data, all three input beams have the same polarization. When the probe beam is cross polarized relative to the grating, the signal drops below the detection limit, indicating that the resonant probe transition is parallel to the excitation ($\Delta\Omega=0$).

III. RESULTS AND ANALYSIS

The absorption spectra of gaseous bromine, aqueous bromine, and bromine isolated in ice are shown in Fig. 2. The visible absorption bands peaking near 400 nm consist of the valence excitations, dominated by the $C(^1\Pi_{1u})\leftarrow X(\Sigma_g^+)$ and $B(^3\Pi_{0u})\leftarrow X$, and a weaker contribution from $A(^3\Pi_{1u})\leftarrow X$.[15] The close proximity of the excited valence potentials and their steep slope in the Franck-Condon region of absorption are responsible for the extensive overlap of these transitions in the spectra. Upon hydration, the peak of the absorption band blueshifts by $\sim$1500 cm^{-1} and broadens. The contributions to the *B* and *C* states, which are clearly visible in Fig. 2(a), coalesce in Figs. 2(b) and 2(c), indicating differential solvation (see Appendix). The hydrated spectra are nearly identical in the solid and liquid phases, suggesting that the spectral perturbations are controlled by the same local structure. In addition, in the hydrated samples, a strong absorption edge appears at $\lambda<300$ nm (see inset to Fig. 2), which is absent in the free molecule. This transition may safely be assigned to the charge transfer states between guest and host.

Attempts at observing fluorescence from hydrated bromine failed. In the case of Br_2 isolated in rare gas matrices, fluorescence over a variety of transitions can be observed: from the ion-pair states at 320 and 345 nm, and vibrationally

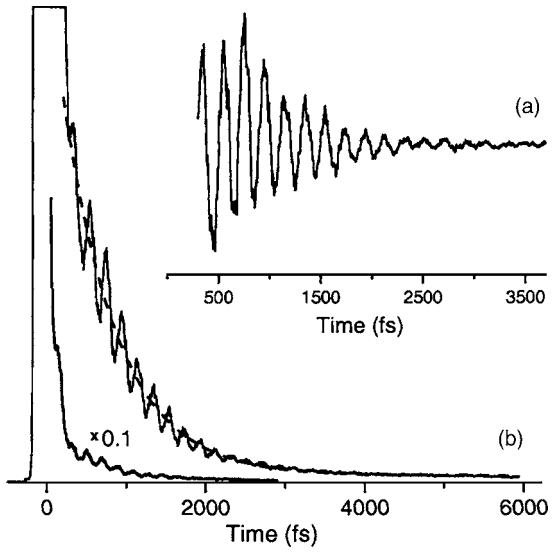

FIG. 3. (a) The transient grating signal showing the evolution of a population prepared at $\lambda_P=550$ nm, along with the single exponential fit to the zero-frequency component. (b) The oscillatory part of the signal obtained after subtraction of the zero-frequency component.

resolved progressions over $B\rightarrow X$ and the overlapping $A\rightarrow X$ and $A'\rightarrow X$ transitions that cover the region from 800 to 1600 nm.[16–19] None of these could be observed in water or ice under a variety of excitation conditions, and for excitation wavelengths ranging from 600 to 350 nm. All fluorescence is strongly quenched in hydrated bromine. In the transient grating experiments, the probe laser at 400 or 405 nm is intended to resonantly probe the B-state population through the molecular ion-pair states. The main ion-pair transitions that are optically coupled to the B state are the $E\rightarrow B$ transition near 310 nm,[20] and the $f\rightarrow B$ transition near 280 nm,[21] in the gas phase. Solvation of the ion-pair states by an estimated 1–1.5 eV of energy would bring these transitions into resonance near 400 nm.[22] The resonance with the ion-pair states is sought for two purposes: (i) sensitivity, due to the large transition dipole of the covalent-to-ionic transitions and (ii) selectivity, to ensure that a well-defined interrogation window along the molecular coordinate projects the ongoing wave packet dynamics.

The transient grating signal obtained for a population prepared at 550 nm and probed at $\lambda=405$ nm is shown in Fig. 3(a). At $t=0$, a response limited nonresonant peak saturates the signal. The noise level due to light scattering is established at negative time, when the probe laser precedes the writing of the grating. The absence of a detectable signal at negative time establishes the limit on electronic dephasing time as $t<120$ fs. At positive time, we observe an exponentially decaying signal that oscillates with a period of ~200 fs. The close correspondence of this period with the harmonic period of $^{79}Br_2(B)$ in the gas phase, $t=199$ fs,[23] allows the inference that a vibrational packet near the bottom of the B potential is being observed. While the depth of modulation of the signal is limited by the time resolution of the measurement, the observation of sharp resonances in time implies a well-defined probe window along the molecular coordinate. Consistent with the absorption spectrum, the upper state of the probe transition may be identified as the solvated molecular ion-pair state. When the probe beam is cross polarized relative to the grating, the signal drops below the detection limit. This polarization dependence indicates a parallel probe transition ($\Delta\Omega=0$), which would be consistent with either $E(^3\Pi_{0g})\leftarrow B(^3\Pi_{0u})$ or $f(^3\Pi_{0g})\leftarrow B(^3\Pi_{0u})$ transitions.

Inspection of the time profile in Fig. 3(a) reveals that the oscillations die out before the completion of the decay of the signal. Accordingly, the signal is fit empirically to

$$S(t)=Ae^{-t/\tau_1}+B\cos(\omega(t-\delta))e^{-t/\tau_2}, \quad (1)$$

where τ_1 and τ_2 represent the decay times of the zero-frequency component and the modulation (with respective amplitudes, A and B), ω is the vibrational frequency of $Br_2(B)$, which can be expected to be time dependent for a damped anharmonic oscillator, and δ marks the appearance time of the first oscillation peak.

The exponential fit to the zero-frequency component, which is shown in Fig. 3(a), yields $\tau_1=750$ fs. The oscillatory part of the signal, after subtracting the zero-frequency component, is shown in Fig. 3(b). The modulation can be adequately fit to a single-frequency damped wave. Since the time origin is established by the nonresonant peak, the fit yields an accurate determination of the time shift: $\delta=134$ fs. Indeed, inspection of the t-zero peak shows a shoulder at $t=134$ fs, confirming the first appearance time. Note, δ longer than the half-period of oscillations necessarily implies that the probe window is located on the right turning point of the potential, and identifies δ as the first half-period of oscillation. Remarkably, the first half-period is ~30% longer than all subsequent oscillations, which show a regular period of ~200 fs. A more detailed description of the modulation is contained in the power spectrum in Fourier domain, which is presented in Fig. 4(a). The spectrum consists of the single peak at 169 cm^{-1}, with noticeable asymmetry. The damping time of oscillations may be characterized by the first moment of the peak. Assuming Lorentzian, the FWHM=17 $cm^{-1}=(\pi c\tau_2)^{-1}$ implies a damping time of $\tau_2=620$ fs, which is meaningfully shorter than the decay of the zero-frequency component, $\tau_1=750$ fs. Though slight, the asymmetry of the spectrum is curious. Bromine has three naturally occurring isotopes, $^{81}Br_2$, $^{79,81}Br_2$, and $^{79}Br_2$, with an abundance of 1:2:1, and harmonic frequencies in the B state of 165.52, 166.57, and 167.61 cm^{-1}, respectively.[23] Given the symmetric abundance, the asymmetry of the spectrum cannot be accounted by the isotopic composition. We are left to believe that the oscillations undergo a frequency sweep (chirp). To obtain the time dependence of the periods of motion, we extract the zero crossings of the wave from its logarithmic plot [see Fig. 4(b)]. The crossings oscillate, indicating that the peaks are broader than valleys, an effect that can be expected from the convolution of the experimental response function (120 fs). The trend of period reduction with time is clearly observed in the plot of the separations between zero crossings [see Fig. 4(c)], the linear fit to which yields a slope of 3 fs/ps (a chirp rate of 2 cm^{-1}/ps). Using this chirp rate, the asymmetry of the spectrum can be adequately reproduced as shown in Fig. 4(a), and contrasted with the best-fit Lorentzian. In the time domain, over the course of the observation,

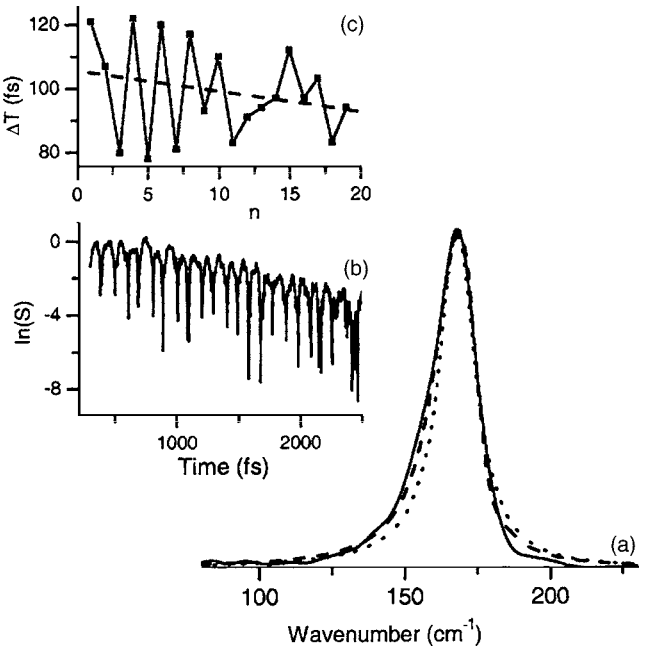

FIG. 4. (a) The power spectrum of the oscillatory component of the signal (solid line), and of simulated signals: $S(t)=B\cos[\omega(t)t]e^{-t/\tau_2}$. The dashed line represents the chirped damped oscillator, where $\omega(t)=\omega_0+\Delta\omega t$ ($\omega_0=165$ cm^{-1}, $\Delta\omega=2$ cm^{-1}/ps, and $\tau_2=650$ fs). The dotted line represents the damped oscillator, where $\omega(t)=\omega_0$ ($\omega_0=168.5$ cm^{-1}, and $\tau_\nu=650$ fs). (b) Semilogarithmic plot of the oscillatory component of the signal allows the determination of zero crossings (negative spikes). (c) The separations between zero crossings vs the index of the crossing show the reduction of period (chirp); the indicated best-fit line has a slope of 3 fs/ps (2 cm^{-1}/ps).

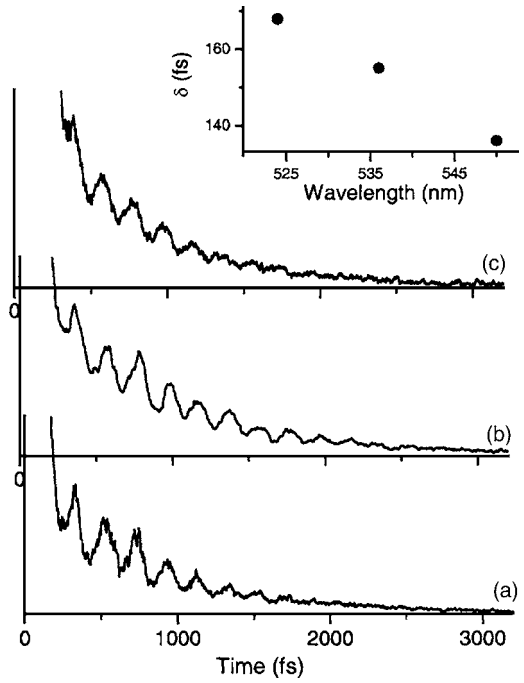

FIG. 5. The transient grating signal probed at $\lambda_{Pr}=405$ nm, and prepared at (a) $\lambda_P=550$ nm, (b) $\lambda_P=536$ nm, and (c) $\lambda_P=524$ nm. The inset shows the first appearance time of the signal as a function of the pump energy.

the oscillation starts with a frequency of 165 cm^{-1} and reaches a terminal value of 169 cm^{-1}, slightly higher than the harmonic frequency of the lightest Br_2 isotope. Given the gas phase anharmonicity of 1.6 cm^{-1}, the observed frequency sweep corresponds to a decay of one vibrational level, from $\nu=1$ to $\nu=0$.

The measurements were repeated at two additional excitation wavelengths, at $\lambda=536$ and 524 nm. The results are compared in Fig. 5. The transients are nearly identical, except for the first appearance time δ, which monotonically increases as the excitation energy increases (see inset to Fig. 5). This is illustrated in the figure by shifting the time origins of the different transients and noting that the oscillations remain in registry. Between 550 and 524 nm, δ stretches from 134 to 168 fs. Otherwise, the power spectra are superimposable, and the Fourier analysis shows the same frequency sweep in the 536 nm data as in the 550 nm data (the 524 nm data is too noisy for a meaningful analysis). Despite the 1000 cm^{-1} range in initial excitation energies, the vibrational wave packet can only be observed to oscillate near the bottom of the potential, and the oscillations are damped within ~600 fs.

To ascertain that the observations are not controlled by the location of the probe window, the full set of measurements was repeated with the probe laser shifted to 400 nm—a shift of 300 cm^{-1}. Since the bond length in ion-pair states is significantly larger (~3.2 Å) than in covalent states (~2.7 Å), blueshifting the probe can be expected to move the window to a shorter internuclear distance, allowing to probe deeper in the B potential. Despite shifting the observation window by 300 cm^{-1}, there is not a discernable effect on the transients within the errors of measurement. Evidently, the damping of oscillations is not due to the packet sliding out of the probe window, but rather due to completion of vibrational relaxation to $\nu=0$. Moreover, since the bottom of the potential is directly observed, the decay of the zero-frequency component of the signal must be attributed to decay of the electronic population out of the B state. Given the radiative lifetime of the B state of 8 μs, we may deduce a fluorescence quantum yield of 10^{-7}—effectively quenched by ice.

In summary, independent of the initial excitation energy and the choice of the probe wavelength, after the first half-period of motion, the vibrational packet appears near $\nu=1$ of the $Br_2(B)$ state in ice. The packet undergoes a frequency sweep while it decays, and reaches a terminal frequency of 169 ± 0.5 cm^{-1}. The oscillatory part of the signal damps out in 620 fs, while the nonoscillatory part decays in 750 fs. The damping of oscillations is to be attributed to relaxation from $\nu=1$ to $\nu=0$, followed by electronic population decay from the stationary $\nu=0$ state. Taking into account the squared dependence of the TG signal on population, we may infer a vibrational relaxation time constant of $\tau_\nu=1240\pm60$ fs and an electronic lifetime of $\tau_e=1500\pm100$ fs.

IV. DISCUSSION

A. Dissipative wave packet motion

In addition to the effective quenching of fluorescence of molecular bromine in ice, efficient vibrational dissipation is revealed. Completion of dissipation, by formation of the stationary $\nu=0$ state, is directly observed. The Fourier analysis

shows a terminal frequency of 169 cm^{-1}, which is $\sim 2\omega_e x_e$ higher than the harmonic frequency of the free molecule ($\omega_e = 166.57$ cm^{-1}, $\omega_e x_e = 1.6159$ cm^{-1}, for $^{79,81}Br_2$) suggesting that the B state is more deeply bound by one vibrational level. The observed chirp of the packet of ~ 3 cm^{-1} corresponds to one vibrational interval. If indeed the chirp is due to vibrational relaxation, then the evolution from $\nu = 1$ to $\nu = 0$ behaves as an underdamped classical anharmonic oscillator. This is unusual. The formation of a wave packet in a quantum oscillator requires the superposition of at least two eigenstates. The superposition of $\nu = 1$ and $\nu = 0$ would oscillate at the highest possible beat frequency $\omega_e - 2\omega_e x_e$ (=164.3 cm^{-1} for the lightest isotope, $^{79}Br_2$, in the gas phase), and its amplitude would decay without change of frequency. Alternatively, the molecular frequency may evolve by adiabatically following a slow coordinate—presumably the cage compression coordinate. In this case, the fact that the observed up chirp corresponds to $\sim 2\omega_e x_e$, would be a pure coincidence. More accurate measurements, along with T dependence, are required to elucidate this unusual observation. In either case, the evolution must be in a vibrational continuum, presumably, due to the soft modes of the ice host that remain effectively coupled to the molecule even near the bottom of its potential.

To contrast the efficacy of the ice bath in accommodating the vibrational energy of the guest, consider the recent pump-probe studies of the same states of bromine isolated in rare gas matrices. In solid Ar, near the bottom of the potential, the $Br_2(B)$ state vibrations retain their discrete nature. This is directly observed in frequency domain spectra, in the form of sharp zero-phonon lines. Also, this is observed in the time domain measurements where beats among the members of a prepared superposition can be observed along with nodal structure and revival times that can be manipulated with chirped pulses. An important difference in the present is that the measurements are carried out at $T = 120$ K, where the thermally populated phonons bridge the vibrational spacing in the molecule.

B. The solvated molecular potential and dissipation during the first half-period

The above considerations concern the directly observed regime of vibrational dissipation. A more dramatic loss of energy can be inferred during the first excursion of the molecular bond. The most direct observation in this regard is that for 1000 cm^{-1} difference in the initial excitation energies, for excitation wavelengths between 550 and 524 nm, the detected wave packet motion is nearly identical—the packet reaches $\nu \sim 1$ after its first half-period of motion. Given the structureless absorption spectrum and its large shift relative to the free molecule, the initial vibrational excitation must be indirectly determined. Under the assumptions that (a) in the measured energy range the potential is represented by the Morse form, and (b) the observed initial appearance time δ represents the half-period of motion at the excitation energy: $2\delta = (\omega c)^{-1}$; the initial vibrational energy may be inferred from the characteristic Morse relation,

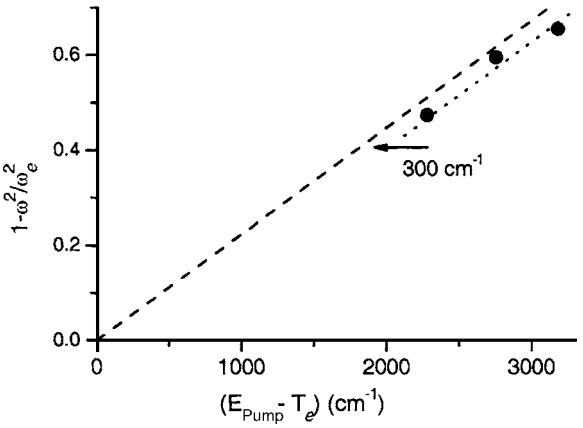

FIG. 6. The $1 - \omega^2/\omega_e^2$ plotted against excitation energy assuming the gas-phase value of the electronic origin T_e. The dashed line represents the same dependence for a gaseous Br_2. The data match the line by upward shifting the origin of the B-potential by 300 cm^{-1}, indicating that the same anharmonicity describes the potential in the gas phase and in ice.

$$1 - \omega^2/\omega_e^2 = (E - T_e)/D_e. \tag{2}$$

In which E is the laser excitation energy, T_e is the electronic origin, and $D_e = \omega_e^2/(4\omega_e x_e)$. Using the experimental harmonic frequency $\omega_e = 169$ cm^{-1}, and the frequency at a given excitation energy, $\omega = (2\delta c)^{-1}$, were we to assume the gas phase values for $T_e = 15\,900$ cm^{-1} and $\omega_e x_e = 1.62$ cm^{-1}, then the three measured points fall on a straight line with a negative intercept, as shown in Fig. 6. The data yield the required zero intercept, and fall in line with the gas phase values when T_e is increased by 300 cm^{-1}. Thus, in the experimental energy range, the B-state potential in ice is characterized as

$$V_B(r) = T_e + D_e[1 - \exp(-\beta(r - r_e))]^2,$$

$$T_e = 16\,200 \text{ cm}^{-1}, \quad D_e = \omega_e^2/(4\omega_e x_e) = 4430 \text{ cm}^{-1},$$

$$\beta = 0.121\,77\omega_e\sqrt{\mu/D_e} = 1.97 \text{ Å}^{-1}, \quad r_e = 2.6776 \text{ Å}. \tag{3}$$

In this one-dimensional representation, a given excitation wavelength leads to a definite initial vibrational energy in the molecule, wherein a dissipation profile may be reconstructed as shown in Fig. 7. An initial fast decay drains most of the

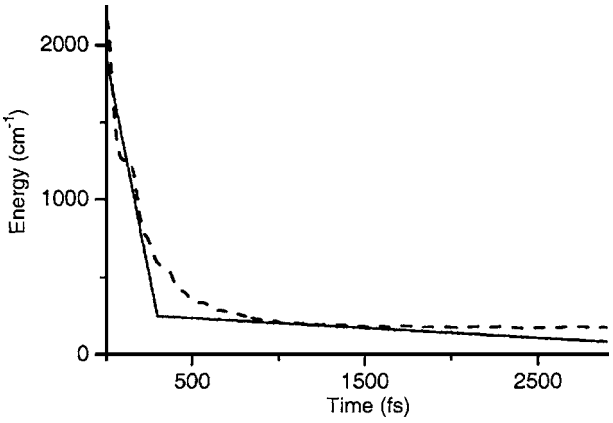

FIG. 7. The reconstructed experimental energy loss along the molecular coordinate (solid line) for a population grating prepared at $\lambda_P = 550$ nm and probed at $\lambda_{Pr} = 405$ nm and the energy loss predicted by 2D simulation (dashed line).

energy, followed by a slower damping of the wave packet as it reaches $v=0$.

C. Guest-host interaction from the absorption spectra

The dynamical analysis above yields the energetics along the intramolecular coordinate, and suggests minor perturbations of the molecular potential. Yet, the absorption spectrum is significantly broadened and shows a blueshift of $\sim 1500\ \mathrm{cm}^{-1}$, of which only $300\ \mathrm{cm}^{-1}$ could be accounted as a shift in the molecular electronic origin. The remaining $1200\ \mathrm{cm}^{-1}$ must arise from the solvent coordinate, energy that must be directly released to the solvent upon excitation. Yet, there is no discernible signature of the solvent dynamics in the observations. Evidently, motion along the solvent coordinate is damped in very short time. We model the system by explicitly considering the solvent coordinate, to reconcile the large solvent induced spectral shift with the absence of any discernible solvent dynamics in the time dependent measurements.

The partitioning of the initial excitation energy between molecular and solvent coordinates can be deduced from the absorption spectrum. Recognizing that the structureless absorption reports on only the short-time correlation between ground and excited state, we may assume separability, to reduce the spectrum to a convolution of spectra along the molecular and solvent coordinates,

$$I(\omega) = \int d\Omega I_1(\omega) I_2(\omega - \Omega), \tag{4}$$

in which the subscripts 1 and 2 refer to intramolecular and intermolecular guest-host (solvent for short) coordinates. To reproduce the observed spectrum, the solvent spectrum $I_2(\omega)$ must consist of a band shifted by $\sim 1000\ \mathrm{cm}^{-1}$, with a FWHM of $\sim 3000\ \mathrm{cm}^{-1}$ (see Appendix). The vertical transition from the equilibrium configuration in the ground state must lead to a significantly repulsive potential along the solvent coordinate. This can be rationalized by considering the energetics of binding between Br_2 and water.

The structure of the $Br_2{-}OH_2$ complex is well established through microwave spectroscopy,[24]

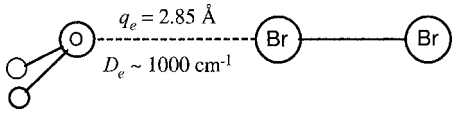

The water binds through the lone pair of electrons on oxygen, to form a collinear O–Br–Br geometry with an O–Br separation of 2.85 Å. *Ab initio* calculations that reproduce the structure predict a binding energy of $1000{-}1250\ \mathrm{cm}^{-1}$, and predict a stretching frequency of $100\ \mathrm{cm}^{-1}$ for the intermolecular stretching coordinate.[25,26] In the 1:1 complex, Br_2 is strongly polarized—while negligible charge is transferred from O to Br, 5% of an electron charge is transferred from the bound Br atom to the free Br atom. The preferred binding to a second water molecule is now via a hydrogen atom approaching the negatively charged Br. This is verified in calculations of $Br_2(H_2O)_n$ clusters, and recognized that the binding energy of the H-bonded water molecules is significantly smaller. Upon the vertical excitation to the B state, an electron is promoted from the nonbonding π orbital to the antibonding σ^* orbital. The increased axial electron density should repel the O-bonded water molecule, while the proton-bound waters may be slightly attracted. Thus, we may suspect that the principle contribution to the perturbation of the absorption spectrum is derived from the single O-bonded water molecule. Indeed, such a local picture must prevail to rationalize the nearly identical spectra of Br_2 in water and ice. We construct a solvent potential guided by the $Br_2{-}OH_2$ interaction. Assuming that the intermolecular distance shifts from 2.85 Å in the ground state to 3.3 Å in the excited state allows the reproduction of the absorption spectrum as detailed in the Appendix.

D. Reconstruction of the time dependent signals

The potentials constructed to reproduce the absorption spectrum are used to simulate the time dependent signals. To this end, in the excited state, we assume a bilinear coupling between the intramolecular r and intermolecular q coordinates,

$$V(q,r) = V(q) + V(r) + \gamma q r, \tag{5}$$

in which $V(r)$ is the $Br_2(B)$ potential [Eq. (3)], $V(q)$ is the potential motivated by the O–Br interaction [Eq. (A2)], and γ is the bilinear coupling constant. Trajectories are computed with initial conditions sampled from a thermal distribution, and subject to a time dependent frictional force,

$$F_q = -\frac{\partial V(q,r)}{\partial q} - \eta_q(t)\frac{\partial q}{\partial t},$$

$$F_r = -\frac{\partial V(q,r)}{\partial r} - \eta_r(t)\frac{\partial r}{\partial t}, \tag{6}$$

with reduced masses $\mu_q = 16$ amu and $\mu_r = 40$ amu, and exponentially damped friction constants η_r and η_q,

$$\eta(t) = \eta_1 e^{-t/\tau}. \tag{7}$$

This form is designed as a convenient means to account for the initial fast decay of energy, without suppressing the amplitude of the classical oscillator near the bottom of the potential. The observable signal is then simulated using a probe window centered at r^* and q^* along the two coordinates,

$$S(t) = \frac{1}{N}\sum_{l}^{N} \exp\left(-\frac{(r(t)-r^*)^2}{\Delta_r^2}\right)\exp\left(\frac{(q(t)-q^*)^2}{\Delta_q^2}\right), \tag{8}$$

where N is the number of classical trajectories, and Δ_r and Δ_q are the widths of the window along molecular and solvent coordinates, respectively. A satisfactory reproduction of the signal (see Fig. 8) and the energy loss profile (see Fig. 7) are obtained, as long as the solvent motion is damped on the time scale of a vibrational period. Several important considerations can be made from the simulations.

(a) The solvent coordinate provides a large dispersion in initial conditions of the trajectories, which in turn leads to dispersion along the molecular coordinate. In the absence of dissipation, the modulation of the signal will be wiped out due to the dispersion of the packet.

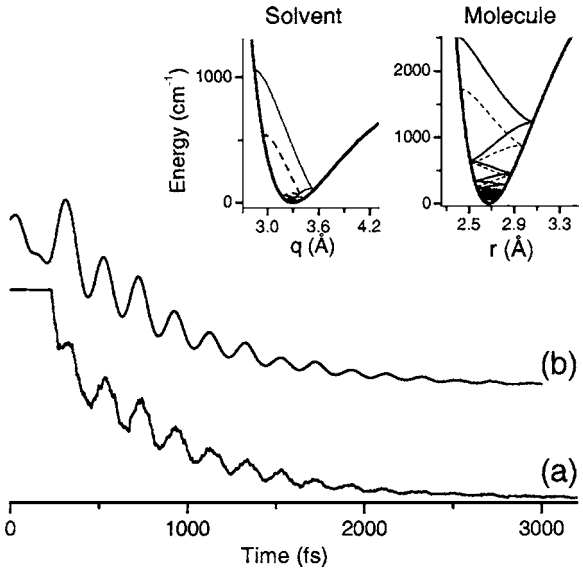

FIG. 8. (a) The signal observed for a population grating prepared at $\lambda_P = 550$ nm and probed at $\lambda_{Pr} = 405$ nm; (b) the simulated signal. The simulation parameters are $\gamma = 2500$ cm^{-1} Å^{-2}, $\eta_r(t) = \eta_1 e^{-t/\tau}$, and $\eta_q(t) = 2\eta_r(t)$ ($\eta_1 = 8$ ps^{-1}, $\tau = 380$ fs), a probe window centered at $(r^*, q^*) = (2.82, 3.3)$ Å and width $\Delta_r = 0.07$ Å and $\Delta_q = 0.25$ Å. The effect of wave packet focusing is illustrated in the inset by two trajectories with different initial partitioning of energies.

By contrast, strong dissipation serves to refocus the spread in the molecular wave packet. This is illustrated in the inset to Fig. 8, in which the energy loss of two trajectories with very different partitioning of energies along the two coordinates is shown.

(b) The first appearance time of the signal δ is controlled by the solvent coordinate, both by the extent of potential coupling [Eq. (5)] and through the modulation of the probe window position. Indeed, the covalent-to-ion-pair resonance, which controls the probe window, should be a strong function of the neighboring water molecule position through dipole-dipole interactions. The observation of a regularly modulated signal can only be reconciled with a solvent coordinate that is already damped. Because of efficient dissipation during the initial stage of dynamics, the assumption that δ measures the half-period at the preparation energy is an oversimplification. Nevertheless, the extracted energetics is not very sensitive to this detail.

(c) When the solvent coordinate is overdamped, the details of the coupling between potentials have little effect on the observable dynamics.

(d) There are two distinct regimes of vibrational dissipation, which in the present is simulated through a time-dependent friction term. The initial dramatic energy loss of 2000–3000 cm^{-1} occurs in $t < 200$ fs, while the subsequent dissipation of ~ 200 cm^{-1} accompanying the damping of the wave packet as it relaxes from $\nu = 1$ to $\nu = 0$ occurs with a time constant of $\tau_\nu = 1240$ fs. Qualitatively similar behavior is well documented in dynamics of caged molecules.[27–29] The extreme cases occur when (i) a Morse oscillator is prepared above its dissociation limit, where a dramatic difference in vibrational energy decay is observed between the first excursion of the bond and subsequent oscillations, and (ii) when strictly cage-bound states are prepared, in which a dramatic change in the first period of motion and subsequent periods is observed.[30] The latter picture is more closely related to the present. Although the molecule is prepared in the deeply bound part of its potential, the solvent coordinate is directly excited.

V. CONCLUSIONS

Fluorescence of Br_2 is strongly quenched in ice. In the specific case of the B state, the electronic population decays in 1.5 ps, reducing its quantum yield of emission to 10^{-7}. The mechanism of electronic quenching must be fairly general, since fluorescence from all known radiative transitions, $D' \rightarrow A'$, $B \rightarrow X$, $A \rightarrow X$, $A' \rightarrow X$, is absent, and the very different coupling matrix elements must be operative in the different states. We surmise that the fluctuating local electric field, due to the orientational disorder of the water molecules, provides electric field gradients of different moments to induce the quenching.

Similarly, very efficient vibrational dissipation is observed through transient grating measurements. Independent of the initial excitation energy, as much as 3000 cm^{-1} of vibrational energy is lost to the host in the first excursion of the molecular bond, to generate a wavepacket near $\nu = 1$. As it damps out, the packet undergoes a frequency sweep that coincides with the loss of one vibrational quantum of energy. A likely interpretation is that the molecular spring adiabatically follows the cage compression coordinate. More accurate and systematic data could greatly help in resolving this uncommon observation. The energy transfer from guest to host shows two regimes, a ballistic mode followed by significantly slower damping near $\nu = 0$. Dissipation and overdamping along the solvent coordinate are key to the observation of a sharply modulated signal, by focusing a packet that would have otherwise been strongly dispersed by the solvent coordinate. This, we illustrated through explicit two-dimensional (2D) simulations of the signal, using potentials that reconcile the strongly perturbed absorption spectra and nearly completely muted solvent contribution in the dynamical measurements. The modeling presumes the interaction with a single O-bonded water molecule to be the principle contribution to the spectral change, with the rest of the ice host acting as an efficient sink of vibrational energy. In the absence of the complex, as would be expected in clathrates, very different spectroscopic and dynamical signatures are to be expected. Work in that direction is in progress.

ACKNOWLEDGMENTS

This work was supported by the U.S. National Science Foundation (Grant No. CHE-0404743). The authors thank Professor N. Schwentner for helpful discussions, as well as Professor V. Mandelshtam for suggestions on data analysis.

APPENDIX

A detailed analysis of the absorption spectra of gaseous Br_2 has been given by Tellinghuisen. To decompose overlap-

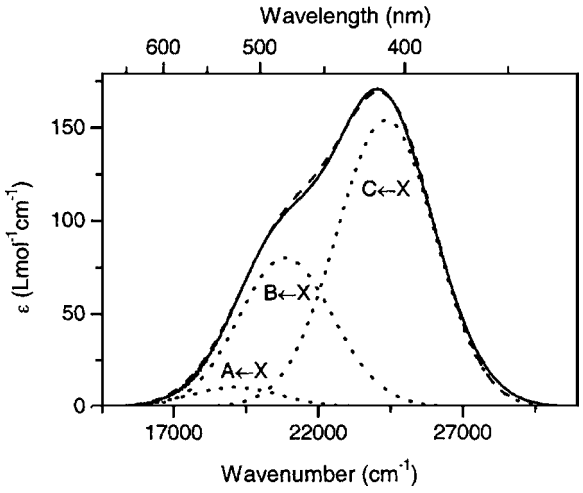

FIG. 9. The decomposition of the experimental absorption spectrum of gaseous Br_2 according to Eq. (A1).

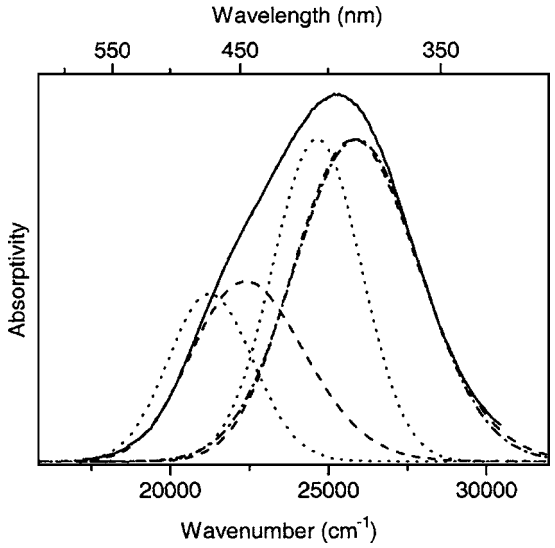

FIG. 10. Absorption spectrum of Br_2 in ice recorded at 120 K (solid line). The decomposition of the spectrum into two spectral components, $C \leftarrow X$ and $B \leftarrow X$ (dashed lines). Also shown are $C \leftarrow X$ and $B \leftarrow X$ absorption bands for a free Br_2 molecule at 120 K (dotted lines) predicted using Eq. (A1). The convolution using Eq. (4) (dot-dashed line) of $C \leftarrow X$ absorption band (dotted line) assuming a Gaussian band shape for the solvent spectrum, with a vertical shift of 1270 cm^{-1} (accounting for 300 cm^{-1} vertical shift of excited-state molecular potentials) and FWHM=3200 cm^{-1} (to simulate $B \leftarrow X$ absorption band in ice the parameters of the solvent spectrum are a shift of 1250 cm^{-1} and FWHM=2800 cm^{-1}).

ping bands, it is more convenient to use an empirical function that describes the shapes of absorption bands and their temperature dependence.[31] It has been shown that three-parameter log normal distribution function approximates well the absorption spectra of halogens,[31,32]

$$\sigma(T) = \sigma_{\max}(T)\exp[-a(T)[\ln(\omega/\omega_{\max})]^2], \tag{A1}$$

where $\sigma_{\max}(T)=\sigma(0)\sqrt{\tanh}$, $a(T)=a(0)\tanh$, and $\tanh=\tanh(\hbar\omega_e/2k_BT)$. In Eq. (A1) the cross section and the wave number at the absorption maximum, $\sigma_{\max}(T)$ and $\omega_{\max}$, and the breadth parameter $a(T)$ are determined by fitting. Provided that the ground state harmonic frequency ω_e is known, $\sigma_{\max}(0)$ and $a(0)$ can be computed, whereas $\omega_{\max}$ does not have temperature dependence in this model. Using Eq. (A1) the absorption spectrum of the gaseous bromine at $T=300$ K can be resolved into three components (see Fig. 9). All three components are well described by Eq. (A1) when compared to Tellighuisen's exact analysis.

We adopt Eq. (A1) to describe the absorption spectrum of bromine in ice. The resolution of the experimentally determined spectrum into two components is shown in Fig. 10. The weakest band in the gas phase, $A \leftarrow X$, is completely buried under the main peak in the solid, which is seemingly a common feature for Br_2 in solution. $C \leftarrow X$ and $B \leftarrow X$ spectral components predicted for the free Br_2 molecule at 120 K are also shown in Fig. 10. To reproduce the experimentally observed blueshift of the overall band, the individual absorption components must be shifted by $\sim$1570 cm^{-1} and broadened by $\sim$1000 cm^{-1}. The absorption spectrum of the hydrated bromine was reconstructed assuming the observable spectrum is a convolution between the spectra along molecular and solvent coordinate [Eq. (4) of text]. It is sufficient to assume a Gaussian line shape for the latter. Good agreement between the experimental and simulated spectra can be achieved if we assume slightly different solvation of the spectral components of Br_2 and take into account the blueshift of Br_2 potentials by 300 cm^{-1} (see Fig. 10).

The spectral contribution from the solvent coordinate can be rationalized in terms of a specific local structure and interaction. Thus, using the known parameters of the Br_2-OH_2 complex, the ground state can be parameterized as a Morse,

$$V(q) = D_e\{1-\exp[-\beta(q-q_e)]\}^2. \tag{A2}$$

In which we use the experimentally known value of $q_e=2.85$ Å, and the theoretically derived values of $D_e=1000$ cm^{-1} and harmonic frequency $\omega_e=100$ cm^{-1}. To represent the excited state, we assume the same potential, but now the minimum moved to $q'_e=3.3$ Å. The thermal population of the ground state along q,

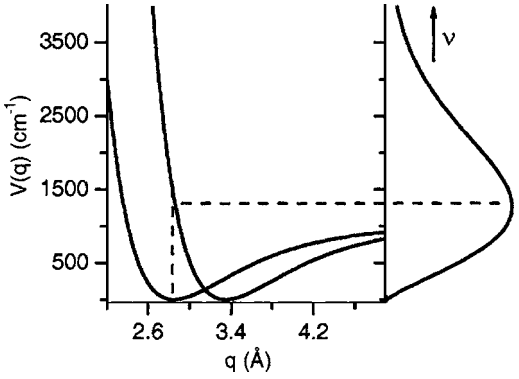

FIG. 11. Potentials of the ground and the excited state of the Br_2-OH_2 binary complex along the intermolecular coordinate (q). The spectrum generated by reflection along this coordinate is shown in the inset to have the shift and width required to reproduce the spectrum of the solvated Br_2 molecule.

$$P(q) = \exp[-V(q)/k_B T'], \tag{A3}$$

is then reflected along q' to generate the solvent spectrum (see Fig. 11). The convolution of this spectrum with the Br_2 spectrum reproduces the experiment.

[1] E. D. Sloan, *Clathrate Hydrates of Natural Gases*, 2nd ed. (Marcel Dekker, New York, 1998).
[2] C. A. Koh, Chem. Soc. Rev. **31**, 157 (2002).
[3] C. Lowig, Mag. Pharm. **23**, 12 (1828).
[4] M. J. Molina, Angew. Chem. **35**, 1778 (1996).
[5] W. R. Simpson, L. Alvarez-Aviles, T. A. Douglas, M. Sturm, and F. Domine, Geophys. Res. Lett. **32**, L04811 (2005); F. Domine, R. Sparapani, A. Ianniello, and H. J. Beine, Atmos. Chem. Phys. **4**, 2259 (2004).
[6] M. S. Gudipati and L. J. Allamandola, Astrophys. J. **615**, L177 (2004).
[7] M. S. Gudipati and L. J. Allamandola, Astrophys. J. **596**, L195 (2003).
[8] V. F. Peterenko and R. W. Whitworth, *Physics of Ice* (Oxford University Press, New York, 1999).
[9] Q.-H. Xu, Y.-Z. Ma, and G. R. Fleming, Chem. Phys. Lett. **338**, 254 (2001).
[10] Q.-H. Xu, Y.-Z. Ma, and G. R. Fleming, J. Phys. Chem. A **106**, 10755 (2002).
[11] S. Fujiyoshi, S. Takeuchi, and T. Tahara, J. Phys. Chem. A **107**, 494 (2003).
[12] M. Gühr, H. Ibrahim, and N. Schwentner, Phys. Chem. Chem. Phys. **6**, 5353 (2004).
[13] M. Gühr and N. Schwentner, J. Chem. Phys. **24**, 123 (2005).
[14] V. A. Apkarian and N. Schwentner, Chem. Rev. (Washington, D.C.) **99**, 1481 (1999).
[15] J. Tellinghuisen, J. Chem. Phys. **115**, 10417 (2001); **118**, 1573 (2003).
[16] V. E. Bondybey, S. S. Bearder, and C. Fletcher, J. Chem. Phys. **64**, 5243 (1976).
[17] J. Langen, K. P. Lodemann, and U. Schurath, Chem. Phys. **112**, 393 (1987).
[18] J. P. Nicolai and M. C. Heaven, J. Chem. Phys. **83**, 6538 (1985).
[19] J. P. Nicolai, J. Vandeburgt, and M. C. Heaven, Chem. Phys. Lett. **115**, 496 (1985).
[20] P. Berwanger, K. S. Viswanathan, and J. Tellinghuisen, J. Mol. Spectrosc. **91**, 275 (1982).
[21] T. Ishiwata, H. Ohyoshi, and I. Tanaka, J. Chem. Phys. **81**, 2300 (1984).
[22] Lowering of ion-pair states possessing is due to solvation of the molecular dipole by the dielectric of the ice host. The stabilization energy can be estimated using the Onsager model of a point dipole μ, isolated in the center of a spherical cavity of diameter d, in a dielectric continuum with dielectric constant ε,

$$\Delta E = -\frac{8(\varepsilon - 1)}{2\varepsilon + 1}\frac{\mu^2}{d^3},$$

for $\varepsilon = 3.2$, $\mu = 12$ D, and $d \sim 6$ Å, a shift of 1.1 eV is to be expected.
[23] R. F. Barrow, T. C. Clark, J. A. Coxon, and K. K. Yee, J. Mol. Spectrosc. **51**, 428 (1974).
[24] A. C. Legon, J. M. A. Thumwood, and E. R. Waclawik, Chem.-Eur. J. **8**, 940 (2002).
[25] I. Alkorta, I. Rozas, and J. Elguero, J. Phys. Chem. **102**, 9278 (1998).
[26] F. Ramondo, J. R. Sodeau, T. B. Roddis, and N. A. Williams, Phys. Chem. Chem. Phys. **2**, 2309 (2000).
[27] R. Zadoyan, M. Sterling, and V. A. Apkarian, J. Chem. Soc., Faraday Trans. **92**, 1821 (1996).
[28] M. Bargheer, P. Dietrich, K. Donovang, and N. Schwentner, J. Chem. Phys. **111**, 8556 (1999).
[29] M. Bargheer, M. Gühr, P. Dietrich, and N. Schwentner, Phys. Chem. Chem. Phys. **4**, 75 (2002).
[30] Z. Bihary, R. Zadoyan, M. Karavitis, and V. A. Apkarian, J. Chem. Phys. **120**, 7576 (2004).
[31] D. Maric and J. P. Barrows, J. Phys. Chem. **100**, 8645 (1996).
[32] R. I. Gray, K. M. Luckett, and J. Tellinghuisen, J. Phys. Chem. A **105**, 11183 (2001).